J Mater Sci (2008) 43:146–154
DOI 10.1007/s10853-007-2131-7

Structure and microstructure of combustion synthesized MgO nanoparticles and nanocrystalline MgO thin films synthesized by solution growth route

K. Venkateswara Rao · C. S. Sunandana

Received: 7 August 2007 / Accepted: 27 August 2007 / Published online: 29 September 2007

Abstract In this work we describe the synthesis, micro structure (XRD, SEM, AFM) of magnesium oxide nanoparticles and magnesium oxide thin films synthesized by urea-based combustion method and solution growth route using magnesium nitrate as the source of Mg. We used fuel-to-oxidizer ratio (Ψ) as a control parameter to investigate how lattice parameter, particle size, and micro strain vary with Ψ = 0.25–2 in the steps of 0.25. Earlier we have studied NiO as a substitutional solute in MgO (Rao KV, Sunandana (2005) Solid State Phys 50:235). The average crystalline size of MgO was estimated from the full width half maximum (Gaussian and lorentzian fits) of the X-ray diffraction peaks using Sherrer's formula and Williamson–Hall plot. The particle size varies from 15(±0.3) nm to 60(±1.2) nm as Ψ is varied systematically. Surface areas of the MgO powders measured using BET method were used to calculate the particle size, which is comparable with the crystalline size calculated from XRD. We also calculated porosity and microstrain in the MgO nanoparticles with varying Ψ. Thin films of MgO are well characterized from XRD and AFM. The size of the particles and RMS roughness of the thin films were calculated using AFM.

K. V. Rao
JNTUCEH, Jawaharlal Nehru Technological University,
Hyderabad 500 085, India

K. V. Rao · C. S. Sunandana (✉)
School of Physics, University of Hyderabad,
Hyderabad 500 046, India
e-mail: csssp75@yahoo.co.in

Introduction

Oxide nanomaterials have a wide range of applications including as catalysts and starting materials for preparing advanced structural ceramics [1, 2]. MgO is highly insulating crystalline solid with NaCl crystal structure with excellent properties such as chemical inertness, electrical insulation, optical transparency, high temperature stability, high thermal conductivity, and secondary electron emission [3]. Magnesium oxide is attractive for both fundamental and applicable research areas [4]. Magnesium oxides are used in a variety of industrial applications, e.g., as heat-resistant and high-temperature insulating materials, and fuel-oil additives [5–7] besides as a heat-resistant glass composite in liquid crystal display panels, electroluminescence display panels, plasma display panels, and fluorescent display tubes [8]. Nanocrystals of common metal oxides such as MgO, CaO, and ZnO have been shown to be highly efficient and active absorbents for many toxic chemicals, including air pollutants, chemical warfare agents [4], and acidic gases. There are several methods for preparing MgO including high-temperature solid state synthesis, sol–gel techniques, and vapor-phase oxidation [9]. In this work, we have explored a relatively new, simple and energy-saving combustion technique for well-optimized synthesis of MgO nanoparticles. The synthesis has been optimized by a systematic variation of fuel/oxidizer ratio (Ψ) and the resulting nanoparticles have been probed for crystalline size, porosity, and microstructure. MgO thin films also find several applications in different developing areas. MgO thin films find application as protective layers in alternative current (AC) plasma display panels (PDPs) because of their low erosion rate and high secondary electron emission coefficient [10, 11]. An alternative dielectric for silicon dioxide (SiO_2) and dynode in electron

multipliers in Zeus display panel. MgO single crystal is an excellent substrate for preparing ferroelectric and superconductor thin films [12]. Recently, there have been a number of studies on the preparation of MgO films deposition by various methods, for example reactive magnetron sputtering [13], pulsed laser deposition [14], ion beam sputtering [15], and plasma enhanced metal organic chemical vapor deposition [16]. In this work, we adopted a novel wet chemical route [17] for preparation of MgO thin films on glass substrates based on a solution containing magnesium (+2) ion and urea and present results on their structure and microstructure.

Samples preparation and experimental techniques

This article has two goals

(1) Synthesis and characterization of nanocrystalline magnesium oxide powder by chemical combustion method.
(2) Fabrication and characterization of nanocrystalline magnesium oxide thin films by solution growth route.

Interestingly, in both methods the starting materials are same, namely magnesium nitrate $Mg(NO_3)_2 \cdot 6H_2O$ and urea (NH_2CONH_2).

Nanocrystalline MgO by chemical combustion

Techniques available for the preparation of nanomaterials are based upon dividing or breaking down a bulk solid or building up processes. Some well-known methods are laser ablation, plasma synthesis, chemical vapor deposition, mechanical alloying or high-energy milling, and sol–gel synthesis [18]. All these techniques are involved, requiring special chemicals and equipment. During the course of our studies, we prepared $Mg_{1-x}Ni_xO$, NiO, and MgO solid solutions by the low-temperature initiated self-propagating, gas producing combustion method [19, 20]. The self-propagating combustion process involves the exothermic reaction of an oxidizer such as metal nitrates, magnesium nitrate, and an organic fuel, typically urea (CH_4N_2O) or carbohydrazide (CH_6N_4O) or glycine ($C_2H_5NO_2$). The mechanism of combustion reaction is quite complex. Parameters that influence the reaction kinetics and mechanism include, type of fuel, fuel to oxidizer ratio, use of excess oxidizer, ignition temperature, and water content of the precursor mixture. For the preparation of the samples of MgO in the present study, the required amount of nitrate $Mg(NO_3)_2 \cdot 6H_2O$ (MERCK Ltd.) was dissolved in distilled water along with fuel urea (NH_2CONH_2) (QUALIGENS). Stoichiometric composition of the metal nitrate and fuel is calculated based upon the propellant chemistry. The heat of combustion is the maximum when the fuel to oxidizer ratio (Ψ) equals to 1 [20]. The fuel to oxidizer ratios (Ψ) [21] are calculated using the below equation,

$$\Psi = \frac{n\{1 * 4_C + 4 * 1_H + 2 * 0_N + 1 * (-2)_O\}}{a\{1 * 2_{Mg} + 2(1 * 0_N + 3 * (-2)_O)\}} \quad (1)$$

where n is mole fraction of fuel and a is the mole fraction of nitrate. We prepared MgO for different fuel to oxidizer ratios Ψ = 0.25, 0.5, 0.75, 1, 1.25, 1.5, 1.75, and 2 by doing stoichiometric calculations as above. The aqueous solution is thoroughly stirred using a magnetic stirrer and placed on a hot plate to initiate the reaction. As the temperature reached 100 °C, water started to boil and evaporate from the solution, which increased solution viscosity substantially, during which the compound caught fire. Finally we are left with light weight white powder which is the precursor. The as-obtained precursor and precursor annealed for 2 h at 300 °C were both characterized. Structural characterization on these samples was performed using Philips X-Ray Diffractometer with Cu–Kα1 radiation. Microstructure studies were carried out using Philips XL-30 SERIES SEM by spreading samples over a well-cleaned microscopic slide after applying vacuum grease. The specific surface area was estimated using N_2 absorption isotherm at 77 K by BET method using an Autosorb-1 instrument (Quanta chrome). AMBIOS XP-1 diamond stylus profilometer was used to measure the thickness of the thin films. To analyze the surface morphology, MgO films were examined by SPA 400 atomic force microscope (AFM) using noncontact dynamic force mode (DFM).

The theoretical equation assuming complete combustion of the redox mixture used for synthesis of MgO is

$$Mg(NO_3)_2 \cdot 6H_2O + NH_2CONH_2 \rightarrow MgO(s) + 8H_2O(g) + CO_2(g) + 2N_2(g) + O_2(g) \quad (2)$$

Nanocrystalline MgO thin films by solution growth route

Preparation of the substrates

For the fabrication of MgO thin films, standard microscope cover glasses were used as substrate. Before thin film deposition float glass slides were cut into 3 cm × 2.5 cm pieces.

They were cleaned subsequently as indicated in steps 1–10 below:

(1) Glass slides were kept for 24 h in sulfochromic acid and cleaned with water;
(2) Warming up to boiling point in 10% soap solution + 90% water;

(3) Removing, withering by rubbing with cotton in cold water;
(4) Warming in chromic acid up to boiling point for removing organic contamination;
(5) Rinsing and washing in cold water to remove surface contaminants;
(6) Ultra-sonification in distilled water for setting down dust particles;
(7) Ultra-sonification in iso-propyl alcohol for 3–5 min duration;
(8) Ultra-sonification in trichloro ethylene for 3–5 min duration to remove greases. The solution becomes whitish in color if substrates were not properly cleaned;
(9) Ultra-sonification in isopropyl alcohol for 3–5 min duration. (No change in color of the solution);
(10) Drying in air before loading into the system for deposition.

Deposition of MgO thin films

The proposed methodology is similar to the [17]. The magnesium oxide films growth is based on thermal treatment of an aqueous solution, which contains magnesium (2+) ions and urea. The deposition bath was prepared by mixing 50 cm^3 1 mol/dm^3 $Mg(NO_3)_2 \cdot 6H_2O$ and 25 cm^3 1 mol/dm^3 urea. Previously prepared substrates were vertically supported against the walls of a 100 cm^3 laboratory beaker. This beaker is kept in oil bath at 100 °C. Upon heating at 100 °C for about 1 h the reaction mixture slowly turned turbid. Within 2 h, the reaction mixture became a white bulk precipitate of $3Mg(OH)_2 \cdot 2H_2O$ settled at the bottom of the beaker. As-deposited films were washed in deionized water and annealed at a temperature of 400–4250 °C for about 48 h. The annealed films were apparently white, uniform, and homogenous. The dependence of the film thickness on the deposition time is shown in the Fig. 1. As can be seen, the deposition practically completed after about 2 h. The terminal thickness is about 2 μm. Thicker films can be prepared by re-immersing the initially deposited thin films into a fresh bath. The overall chemical reaction of the deposition process may be expressed with the following equation

$$3Mg^{2+} + 2NH_2CONH_2 + 10H_2O = 3Mg(OH)_2 \cdot 2H_2O + 4NH_4^+ + 2CO_2 + 2H^+ \quad (3)$$

The chemistry of the deposition process is based on the fact that urea decomposes to CO_2 and NH_3 by heating at higher temperature (90–100 °C).

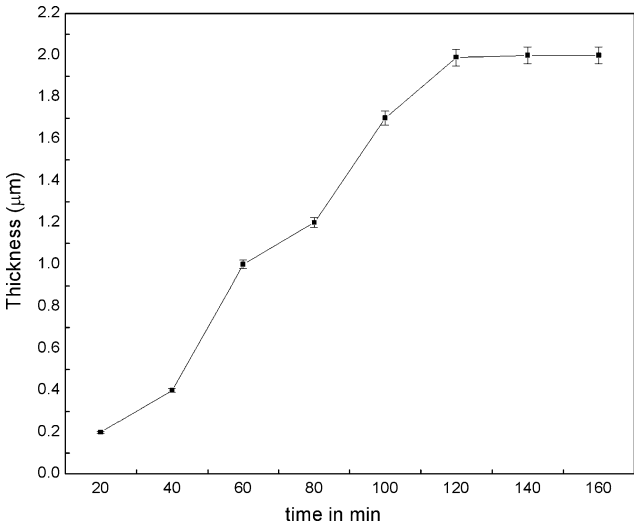

Fig. 1 The dependence of the film thickness on the deposition time in minutes

Results and discussion

X-ray diffraction of chemical combustion synthesized MgO

X-ray diffraction patterns indicate that the monophasic fcc MgO phase is obtained by annealing precursor at 300 °C for fuel to oxidizer ratio ψ = 0.75–2 in the steps of 0.25. For Ψ = 0.25 and 0.5, two phases MgO and $Mg(OH)_2$ arise due to insufficient heat generated during combustion resulting in residual moisture in the sample mixture. The intensities of (111), (200), (220), (311), and (222) XRD peaks are comparable with JCPDS (78-0430) values as shown in Fig. 2. Lattice parameters are almost coincident for all the fuel to oxidizer ratios (Ψ) (in good agreement with JCPDS) but, as the size of the particle or crystalline size is decreasing there is a small contraction in the lattice parameter. Thus systematic variation of the lattice parameter versus crystalline size is observed. The contraction of lattice parameter with decrease of the crystalline size suggests that surface tension probably plays a major role in determining the lattice parameter [22]. The surface-free energy of a nanocrystal arises from the surface chemical bonds created during formation. The total surface energy is the product of the number of surface chemical bonds and the surface bond energy [23]. The surface energy increase of nanoparticles will tend to contract their sizes by distorting their crystal lattice elastically. Of course, this kind of distortion is very small compared to the whole particle size.

Crystallite size

All samples produce appreciable diffraction broadening and it is reasonably assumed that this arises from the

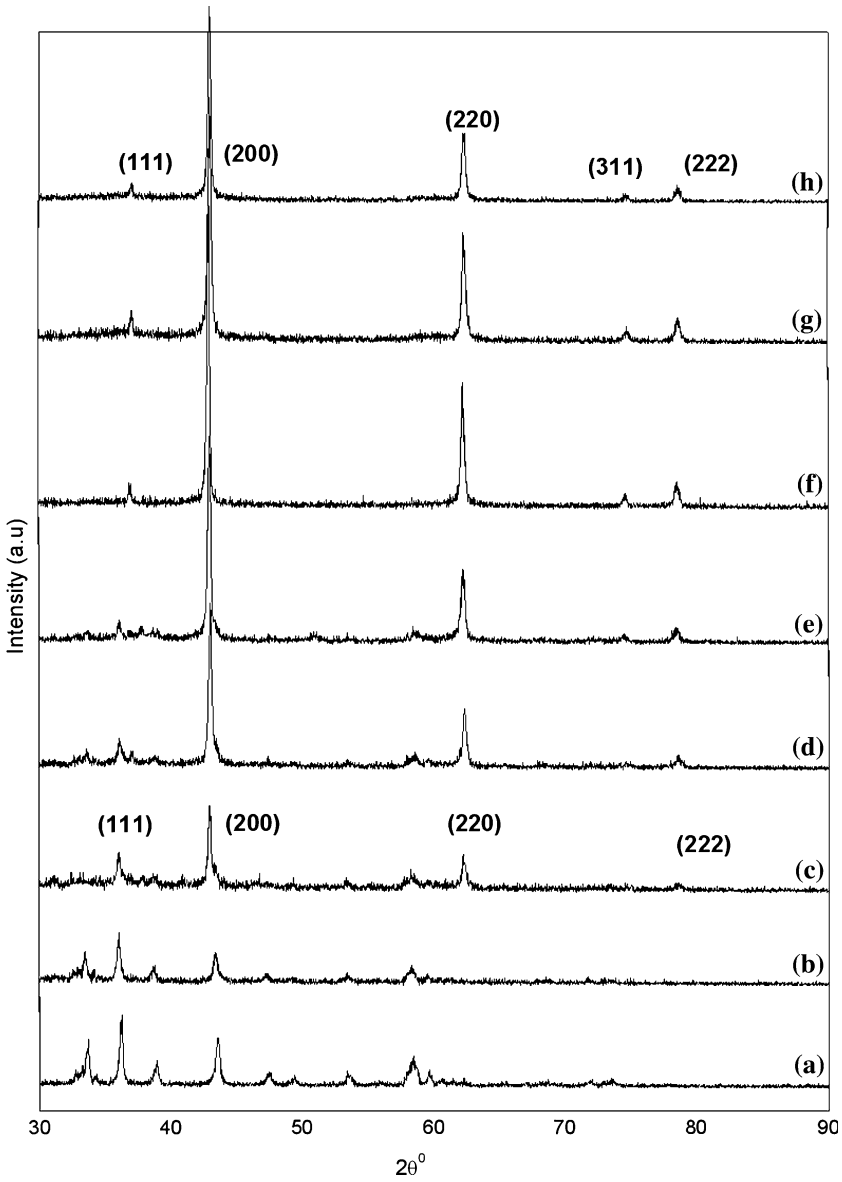

Fig. 2 Room temperature XRD patterns of MgO nanoparticles prepared by chemical combustion with different fuel to oxidizer ratios (ψ) (**a**) $\psi = 0.25$, (**b**) $\psi = 0.5$, (**c**) $\psi = 0.75$, (**d**) $\psi = 1$, (**e**) $\psi = 1.25$, (**f**) $\psi = 1.5$, (**g**) $\psi = 1.75$, (**h**) $\psi = 2$

crystalline and internal stresses. Diffraction theory predicts that the breadth due to crystallite size varies with angle as sec θ and that due to elastic strain as tan θ [24]. The additional broadening in diffraction peaks beyond the inherent peak widths due to instrumental effects can be used to measure crystallite sizes as low as 1.0 nm .The crystallite size of prepared and annealed compositions were calculated from the full width at half maximum (FWHM) of all the peaks (111), (200), (220), (311), and (222) using the Debye–Scherrer formula [25]

$$t = \frac{0.9\lambda}{w\cos\theta} \tag{4}$$

Use of the Gaussian function and Lorentzian function to fit the FWHM of all the peaks yields more accurate results.

We also used another procedure based on the Williamson–Hall equation to calculate strain and particle size of the each sample [26]. The Williamson–Hall equation is

$$B\cos\theta = \frac{K\lambda}{t} + 2\varepsilon\sin\theta \tag{5}$$

where B is the full width at half maximum (FWHM) of the XRD all peaks, K is Scherrer constant, t is the crystalline size, λ the wave length of the X-ray, ε the lattice strain, and θ the Bragg angle. In this method, $B\cos\theta$ is plotted against $2\sin\theta$. Using a linear extrapolation to this plot, the intercept gives the particle size $K\lambda/t$ and slope gives the strain (ε). Here, as we vary the fuel to oxidizer ratio the average size of the particle is varied from 15(±0.3) nm to 60(±1.2) nm as shown in Fig. 3. The heat of combustion is maximum for $\Psi = 1$ [21], and hence the size of the particle is

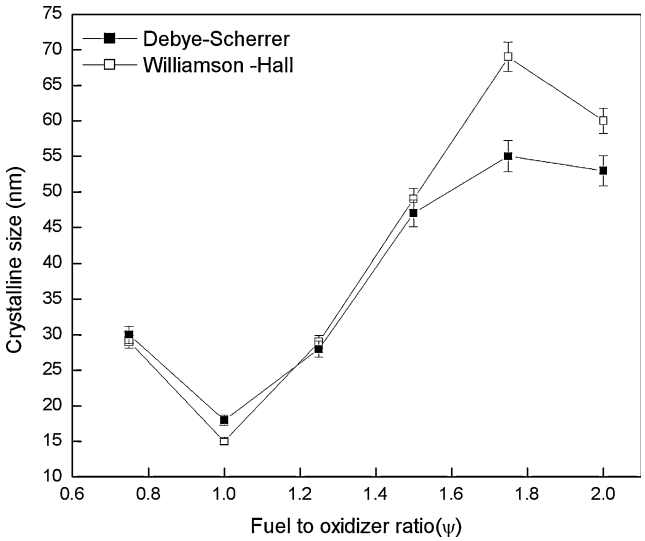

Fig. 3 Average crystalline size of the MgO powders prepared by chemical combustion are calculated from Debye–Scherrer formula and Williamson–Hall plot

minimum for $\Psi = 1$ and as Ψ increases from 0.75, the size of the particle is decreased till $\Psi = 1$ and then it is increased. This can be explained as due to differences in ignition temperature, burn rate and adiabatic flame temperatures and enthalpies resulting from systematic changes in the thermodynamic conditions and the properties of the gas(es) evolved thereof. For $\psi = 1$ the above parameters are probably optimized to produce the smallest particles. The same phenomenon was observed by us earlier in the preparation of NiO [27].

Measurement of surface area

The specific surface area measurement is one of the important parameters used to characterize powder samples and it is related with other parameters, such as particle size, shape, and density. The specific surface area of MgO samples prepared by combustion processes were measured by using Brumauer Emmett Teller (BET) equation [28] which describes the physical absorption of gas (nitrogen) on a solid is utilized in obtaining the specific surface area. The specific surface area is maximum when $\Psi = 1$ and while for Ψ less then or greater then 1 it decrease. It is the consequence of mechanical-free energy changes with Ψ. The particle size is given by

$$D = \frac{6 \times 10^3}{S \cdot \rho} \tag{6}$$

where S is the specific surface area and ρ is the density of MgO (3.58 g/cm^3) [29]. From a perusal of Table 1, one can infer that the particle size is comparable with the crystalline size which is calculated in Debye–Scherrer and Williamson–Hall plot methods.

Table 1 The crystalline size calculated from XRD using Debye–Scherrer formula and Williamson–Hall plot are comparable with particle size calculated from specific surface are (BET)

Ψ	Debye–Scherrer crystalline size (nm)	Williamson–Hall crystalline size (nm)	Particle size from BET surface area (nm)
0.75	30 ± 1.5	29 ± 0.58	28 ± 0.56
1	18 ± 0.9	15 ± 0.3	12 ± 0.24
1.25	28 ± 1.4	29 ± 0.58	29 ± 0.58
1.5	47 ± 2.4	49 ± 1	46 ± 0.9
1.75	55 ± 2.8	69 ± 1.4	62 ± 1.2
2	53 ± 2.7	60 ± 1.2	55 ± 1.1

Micro strain

Micro strain in the system is calculated using the Williamson–Hall plot equation. By seeing the Table 2, micro strain is maximum when the average particle size is minimum, that is, for $\Psi = 1$. The micro strain is decreasing when the Ψ is increasing and decreasing as shown in the Table 2. This could be because the mechanical surface-free energy of the metastable nanoparticles is probably maximized for $\Psi = 1$. As the size decreases the lattice parameter probably contracts thereby increasing micro strain in the samples.

X-ray diffraction of thin films of MgO

The results of X-ray diffraction in as-prepared and annealed MgO thin films are shown in Fig. 4. As can be seen, the annealing process influences the film structure of MgO. Also, an increase of the degree of the crystallinity of the MgO is observed upon annealing. The observed diffraction peaks are in a very good agreement with the standard values of JCPDS (78-0430). The MgO has a cubic (NaCl-type) structure with lattice parameter 0.4225(±0.008) nm. Using the Debye–Scherrer and Williamson–Hall formula using

Table 2 Micro strain of the combustion synthesized MgO samples with different Ψ

Ψ	Micro strain $\times(10^{-4})$
0.75	7.39 ± 0.22
1	32.5 ± 0.97
1.25	28.3 ± 0.84
1.5	26.9 ± 0.80
1.75	25.2 ± 0.75
2	5.35 ± 0.16

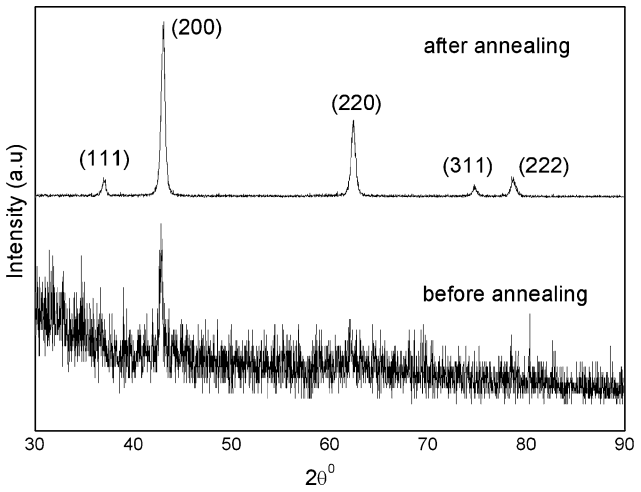

Fig. 4 Room temperature X-ray diffraction of the as-deposited and annealed thin films of MgO

the full width at half maximum intensity of the XRD peaks, we have calculated the average crystalline size. It varies from 24(±0.48) nm to 27(±0.54) nm.

Table 3 Porosity of the MgO powder calculated from XRD

Ψ	Porosity
0.75	0.5084 ± 0.015
1	0.0416 ± 0.001
1.25	0.0558 ± 0.001
1.5	0.0866 ± 0.002
1.7	0.0224 ± 0.0006
2	1.4492 ± 0.0434

Porosity measurement

Generally products of combustion synthesis are highly porous due to evolution of gases in the processes involved .Thus they possess much less densities compared to theoretical values [30]. The porosity of the annealed samples was determined by the X-ray spectrum. The percentage of porosity was calculated from the measured and theoretical density, according to the following equation

$$\text{Porosity}\,(P) = (1 - \frac{D}{D_{\mathrm{T}}})100 \tag{7}$$

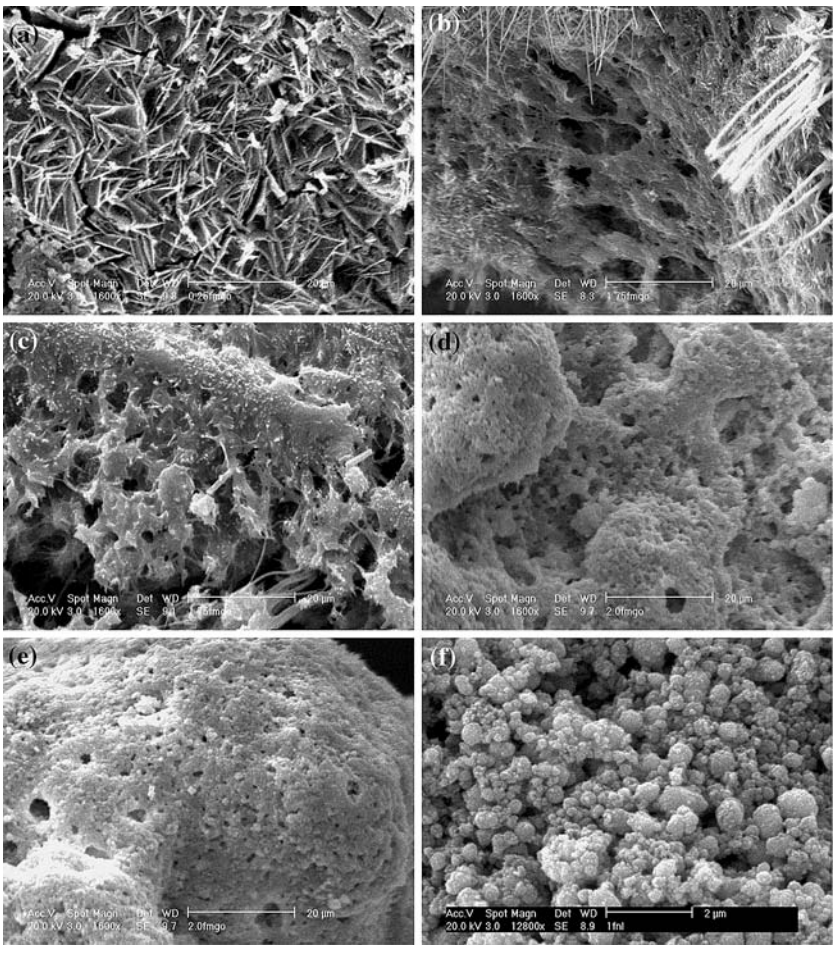

Fig. 5 Scanning electron micrographs shows the microstructure of MgO particles at room temperature. (**a**) ψ = 0.25, (**b**) ψ = .75 (**c**) ψ = 1.5, (**d**) ψ = 1.75, (**e**) ψ = 2, (**f**) ψ = 1 the powder of MgO particles are ultrasonificated in toluene

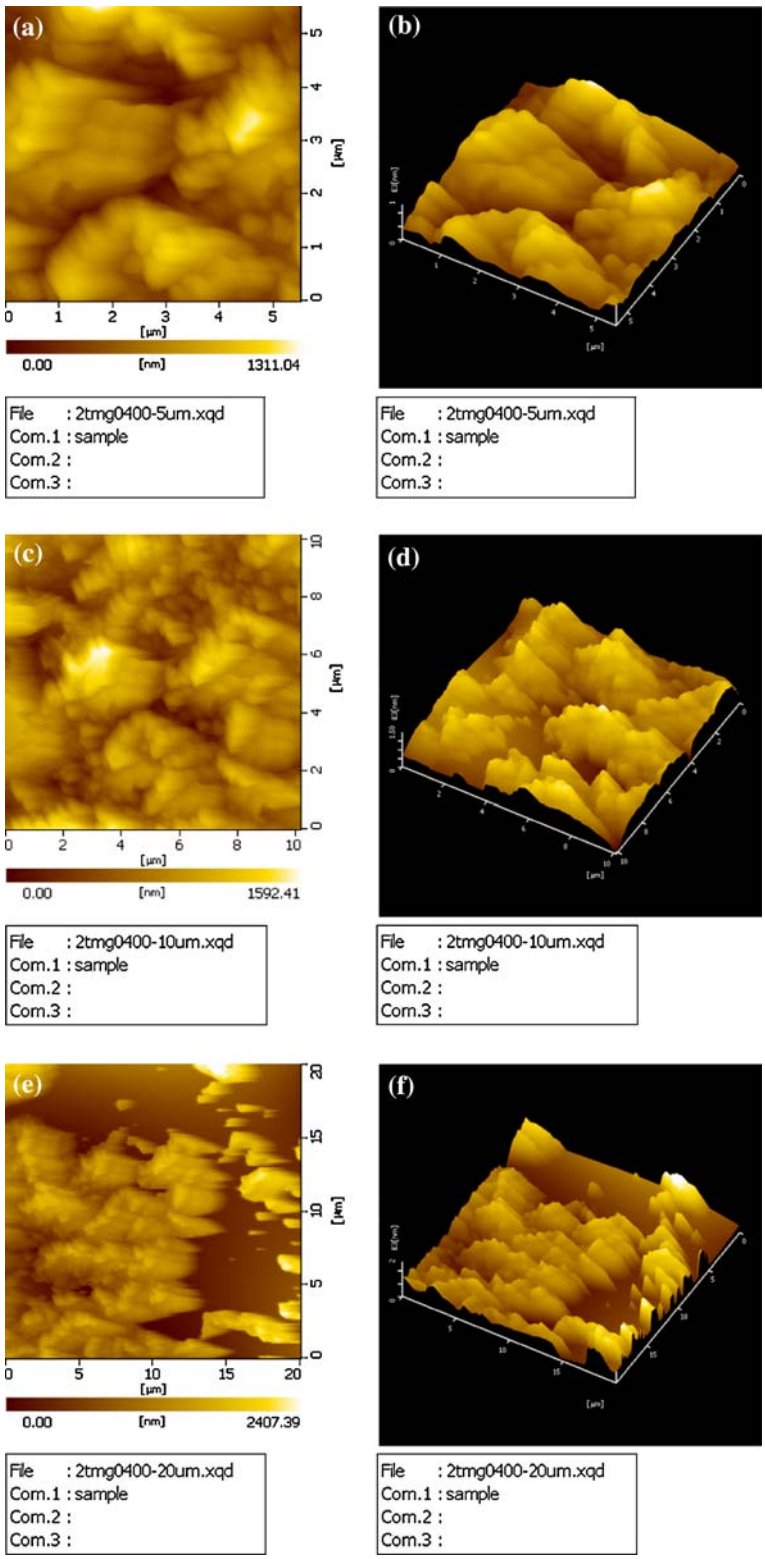

Fig. 6 AFM images of the MgO thin film (sample 1) with scan area (**a**) 5,000 × 5,000 nm^2 (2-D view), (**b**) 5,000 × 5,000 nm^2 (3-D view), (**c**) 10,000 × 10,000 nm^2 (2-D), (**d**) 10,000 × 10,000 nm^2 (3-D) (**e**) 20,000 × 20,000 nm^2 (2-D), (**f**) 20,000 × 20,000 nm^2 (3-D)

where D_T is theoretical density. The calculated porosity values are presented as in Table 3. The porosity first decreases as the Ψ increases and after $\Psi = 1$ the porosity is increased because the excess fuel to oxidizer ratio leads to the progressive evolution of gases. In case of the MgO thin films the percentage of the porosity is 0.88 ± 0.01, which is small when compared to the combustion-produced MgO material. The SEM micrographs provide visual proof for increasing the porosity.

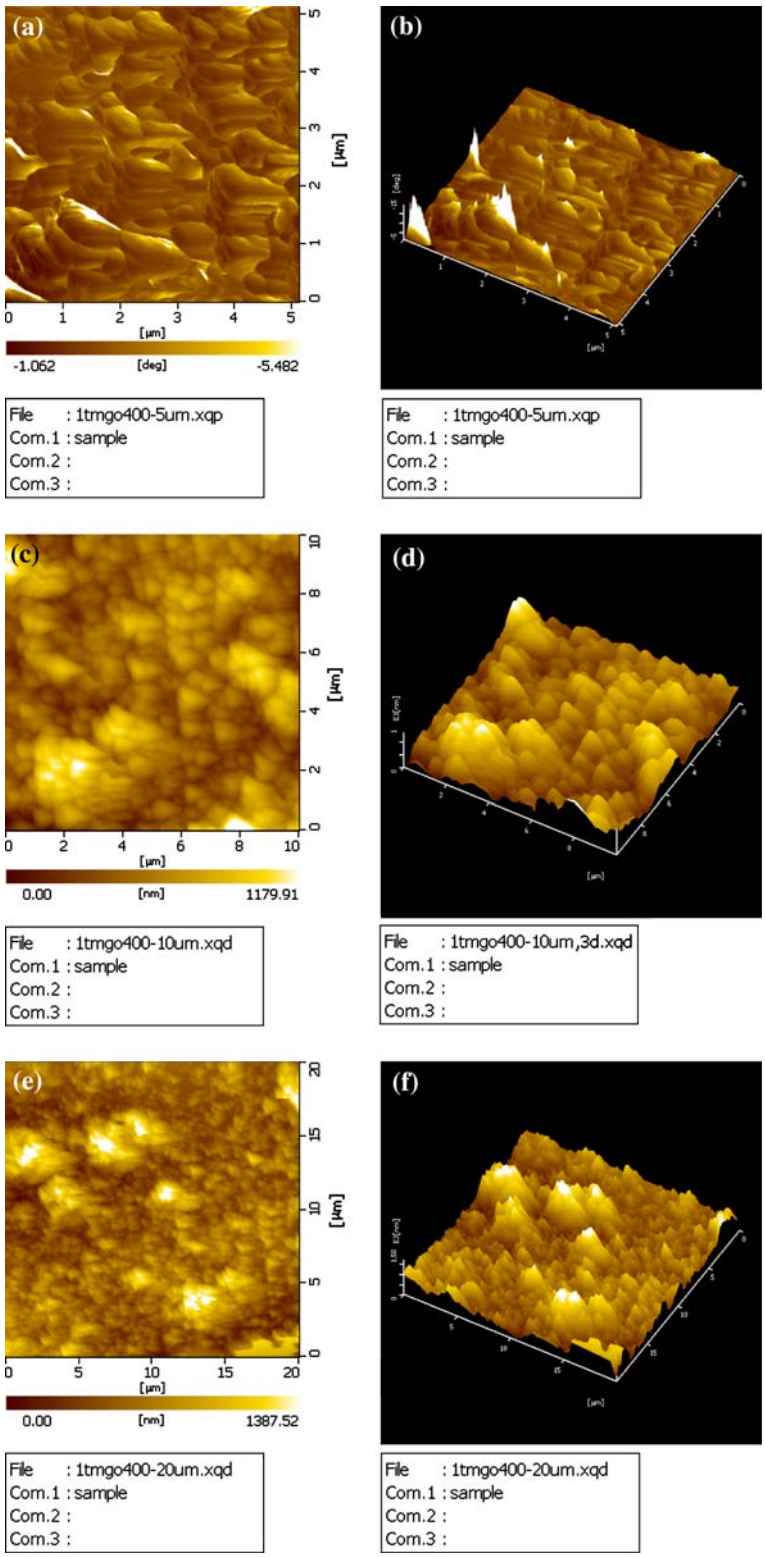

Fig. 7 AFM images of the MgO thin film (sample 2) with scan area (**a**) 5,000 × 5,000 nm^2 (2-D view), (**b**) 5,000 × 5,000 nm^2 (3-D view), (**c**) 10,000 × 10,000 nm^2 (2-D), (**d**) 10,000 × 10,000 nm^2 (3-D) (**e**) 20,000 × 20,000 nm^2 (2-D), (**f**) 20,000 × 20,000 nm^2 (3-D)

Scanning electron microscope studies

The SEM micrographs of combustion synthesized MgO powders are shown in Fig. 5. These powders of MgO show increase in the porosity as expected due to the excess of fuel corroborating to the values of the porosity calculated from XRD. As the fuel to oxidizer ratio is increasing, the porosity is increasing in Fig. 5a ($\Psi = 0.25$), Fig. 5b ($\Psi = .75$), Fig. 5c ($\Psi = 1.5$), Fig. 5d ($\Psi = 1.75$), and Fig. 5e ($\Psi = 2$), respectively. We ultra-sonicated the MgO

powders in toluene for 10 min to disperse the particles and the SEM micrograph is as shown in Fig. 5f. Due to ultrasonication, we could get uniform and spherical particles of average grain size which vary from 300 nm to 350 nm.

AFM

In order to get a direct morphological view of the thin films MgO nanoparticles and to estimate the distribution of the particle sizes and RMS roughness, AFM seems to be the ideal probe. The AFM micrographs are shown in the Figs. 6 and 7. In Figs. 6 and 7, two samples of MgO thin film at different scan areas $5{,}000 \times 5{,}000$ nm^2, $10{,}000 \times 10{,}000$ nm^2, and $20{,}000 \times 20{,}000$ nm^2 are shown in two and three dimensions. From a careful examination of AFM micrographs, one can observe columns elongated along a preferential growth direction and agglomeration of grains with some truncated cone like growth are seen. These dome-shaped grains having different sizes vary from 55 nm to 250 nm. The size of the particles varies from 250 nm to 520 nm. The RMS roughness of the samples is varying from 203 nm to 350 nm. We can conclude from these observations that it is possible to make MgO thin films with controlled size and roughness in a simple synthesis procedure.

Conclusions

we synthesized MgO nanoparticles size 15(±0.31) nm to 60(±1.2) nm, varying fuel to oxidizer ratio $\Psi = 0.75$–2 in the steps of 0.25. We also synthesized MgO nanocrystalline thin films by solution growth route with same starting materials. Surface area of the combustion synthesized MgO nanoparticles were measured using BET. From the surface area the size of the particles calculated is comparable to the crystalline size that was calculated from XRD. We determined the micro strain in the combustion synthesized MgO using Williamson–Hall plot, the strain is maximum for $\Psi = 1$ and it is decreased as the Ψ is increased. Porosity of the MgO is increased with increase in Ψ, the same is observed in SEM micrographs. Thin films MgO are characterized by XRD and AFM. The thickness of the films increases with time. The crystalline size of the MgO thin films are varying from 24(±0.48) nm to 27(±0.54) nm. The porosity of the thin films is less when compared to combustion synthesized MgO. The RMS roughness of the thin films samples are varying from 203 nm to 350 nm which is measured from AFM.

Acknowledgments K. V. Rao thanks the JNT University and Department of Physics, JNTU College of Engineering, Hyderabad for encouragement. We thank Dr .K. V. R. Chari, IICT Hyderabad for help in BET surface area measurements.

References

1. Rao KV, Sunandana CS (2005) Solid State Phys (India) 50:235
2. Park J-Y, Lee Y-J, Jun K-W, Aeg J-O, Yim D-J (2006) J Ind Eng Chem 12(6):882
3. Durusory HZ (1991) J Mater Sci Lett 10:1023
4. Wagner GW, Bartram PW, Koper O, Klabunde KJ (1999) J Phys Chem B103:3225
5. Poullikkas A (2004) Energy Convers Manage 45:1725
6. Guo XL, Chen ZG, Zhu SN, Xiong SB, Hu WS, Lin CY (1996) J Appl Phys 29:1632
7. Li YR, Liang Z, Zhang Y, Zhu J, Jiang SW, Wei XH (2005) Thin Solid films 489:245
8. Brien JC (1982) J Inst Energy 15:115
9. Itatani K, Yasuda R, Howell FS, Kishioka A (1997) J Mater Sci 32:2977, doi:10.1023/A:1018649222749
10. Boeaf JP (2003) J Phys D Appl Phys 36:R53
11. Byrum BW Jr (1975) IEEE Trans Electron Devices ED-22(9):685
12. Phillipsa Julia MA (1996) Appl Phys 79:1829
13. Pan C, O'Keefe P, Kester JJ (1998) SID98 Digest 29:865
14. Ishiguro T, Hiroshima Y, Inoue T (1996) Jpn J Appl Phys Pt 1 35(6):3537
15. Ishihra T, Motyamam M (1986) J Ceram Soc Jpn 97:771
16. Fujii E, Tomzawa A, Fujii S, Torii H, Takayama R, Hiro T (1994) Jpn J Appl Phys Pt 1 33(11):6331
17. Biljana P, Tanja K, Metodija N, Ivan G (2000) Appl Surf Sci 165:271
18. Siegel RW (1993) Mater Sci Eng A 168:189
19. Mimani T, Patil KC (2001) Mater Phys Mech 4:134
20. Arul Dhas N, Patil KC (1992) Int J Selfpropag High Temp Synth 1:576
21. Kingsley JJ, Patil KC (1988) Mater Lett 6:427
22. Morris VN, Farrell RA, Sexton AM, Morris MA (2006) J Phys Conf Ser 26:119
23. Ragone DV (1995) Thermodynamics of materials, chapter 4, vol II. John Wiley & Sons Inc
24. Wilson ACJ (1962) X-ray optics, 2nd edn. Lone, Methune
25. Cullity BD (1978) Elements of X-ray diffraction. Addison-Wesely Publishing Company, Inc., Philippines
26. Kameli P, Salamati H, Aezami A (2006) J Appl Phys 100:053914
27. Rao KV, Sunandana CS (2007) Advanced nano materials 2007 international conference. IITBOMBAY, India, p 112
28. Brumauer S, Emmeteof PH, Teller E (1938) J Am Chem Soc 60:309
29. Robert CW, Melvin JA, Willian HB (1986) The CRC hand book of chemistry and physics, 66th edn. CRC press, Boca Raton, FL
30. Bhaduri SB, Bhaduri S (1999) Non equilibrium processing of materials. Amsterdam Publication, p 289